Appl. Phys. A (2016) 122:878
DOI 10.1007/s00339-016-0397-9

Applied Physics A
Materials Science & Processing

Aluminum- and boron-co-doped ZnO ceramics: structural, morphological and electrical characterization

Shimin Liu[1] · Jindong Liu[1] · Weiwei Jiang[1] · Chaoqian Liu[1] · Wanyu Ding[1] · Hualin Wang[1] · Nan Wang[1]

Received: 18 June 2016 / Accepted: 24 August 2016 / Published online: 8 September 2016

Abstract Highly dense and electrically conductive aluminum- and boron-co-doped ZnO (ABZO) ceramics were prepared by traditional pressureless sintering process. Single aluminum-doped ZnO (AZO) ceramics were synthesized with similar process and characterized for comparison. The densification behavior, crystal structure, morphology, composition and electrical properties of the ceramics were studied. Results indicated that AZO ceramics with the maximum relative density of 99.01 % were obtained only at 1350 °C for 4 h, which, however, was accompanied by electrical conductivity deterioration because of the increased insulated $ZnAl_2O_4$ phase formed in ceramics. Interestingly, the ABZO ceramics reached the maximum relative density of 98.84 % at 1100 °C, which was 250 °C lower compared with that of AZO ceramics. Moreover, the electrical conductivity of ABZO ceramics improved significantly with the increased sintering temperature and increased insulated $ZnAl_2O_4$ phase, which should be ascribed to the decreased grain boundaries and the resultant reduced carrier scattering in ceramics overcoming the influence of increased $ZnAl_2O_4$ phase due to boron doping effect.

1 Introduction

ZnO is an important *n*-type II-VI group semiconductor with a wide band gap of 3.37 eV at room temperature [1]. When doped with group III elements including Ga [2], Er [3], In [4] and Al [5–19], the electrical resistivity of ZnO decreases exponentially. Aluminum-doped ZnO (AZO) has been extensively studied for optoelectronic applications because it concurrently exhibits low electrical resistivity, high optical transparency, good thermal stability and low cost [6–8]. Commercially, transparent conductive AZO films are produced from AZO ceramic sputtering technique [9–12]. Sputtering technique has advantages of high deposition rate, good film adhesion and low temperature substrate. It is noteworthy that AZO ceramics with high relative density and low electrical resistivity are urgently needed to obtain AZO films with few structural defects and necessary specifications [13, 14].

Several methods have been developed for preparing AZO ceramics. Now, AZO ceramics with the relative density of ~98 % have been obtained using hot pressing (HP) and hot isostatic pressing (HIP) methods by adding sintering aids [15, 16]. Neves et al. [17] obtained AZO ceramics with the relative density of ~99 % from AZO nanostructured powders. Chen et al. [18] obtained AZO ceramics with relative density of 99.4 % using SPS method at a high heating rate of 100 °C/min. Wu obtained AZO ceramics with nearly full density using cold isostatic pressure technique based on the two-step sintering process [19]. Among the above reports, however, the formation of insulated $ZnAl_2O_4$ phase in ZnO matrix with sintering temperature is still the severe problem to hinder the electrical conductivity and relative density of AZO ceramics. To our knowledge, a facile sintering process has not been employed for preparing AZO ceramics with simultaneous good electrical property and high relative density. Therefore, it is worth seeking a patentable process under mild conditions for such particular purposes.

✉ Shimin Liu
lsm@djtu.edu.cn

[1] Engineering Research Center of Optoelectronic Materials and Devices, School of Materials Science and Engineering, Dalian Jiaotong University, Dalian 116028, China

Boron-doped ZnO (BZO) could generate free electron carriers, which can therefore increase the carrier concentration and contribute to the electrical conductivity of ZnO [20]. At the same time, it is reported that B^{3+} has high value of Z/r_R^2, which will polarize the electron cloud of the O $2p^6$ valence strongly, thereby increasing the Hall mobility and reducing the electrical resistivity of ZnO [21]. In the present study, aluminum- and boron-co-doped ZnO (ABZO) ceramics simultaneously with high dense and good electrical conductivity were obtained. The densification behavior, crystal structure, morphology, composition and electrical resistivity of the ceramics have been investigated and discussed. For the sake of comparison, the single aluminum-doped ZnO (AZO) ceramics were prepared and characterized.

2 Experimental

2.1 Preparation

Commercial ZnO, Al_2O_3 and H_3BO_3 powders (purity >99.9 %) were used as starting materials without further purification. Firstly, 1.5 wt% ammonium polyacrylate (analytical grade) was added into the distilled water (5 MΩ cm). A specified amount of ZnO and Al_2O_3 powders were mixed with H_3BO_3 powder in the above aqueous ammonium polyacrylate dispersant solution. The powder content in the above ABZO slurry mixture was 55.5 wt%. The Al concentration in ABZO powder was 1.6 at. % [Al: (Al + B + Zn)], and B concentration in ABZO powder was 0.5 at. % [B: (Al + B + Zn)]. The mixture was then gently ball-milled for 48 h. Next, 1 wt% polyacrylic emulsion (analytical grade) was mixed with the above white slurry. The amounts of the dispersant (1.5 wt%) and the binder (1 wt%) were based on the weight of the total dry powder. The mixture was further ball-milled for 0.5 h and then dried at 150 °C to complete dehydration using a spray dryer (S-1500, Sunyitech Co., China). The obtained dry powders were cold-compacted under 28 MPa by uniaxial press and subsequently cold isostatic-pressed (CIP) under 250 MPa to further enhance the green density. The relative density of pressed green bodies was 62.2 ± 0.7 % of theoretical density (5.61 g/cm^3). The final dimension of the pressed cylindrical specimen was 57.1 ± 0.2 mm in diameter and 8.9 ± 0.04 mm in thickness. Afterward, the green bodies were sintered in an air furnace at a heating rate of 100 °C/h. Finally, the specimens were cooled to room temperature naturally. The similar synthesis of AZO ceramics without H_3BO_3 was also performed. The Al concentration in AZO starting powders was 1.6 at. % [Al: (Al + Zn)].

2.2 Characterization

The relative density of green bodies was obtained by measuring the dimension and weight (geometric density). The relative density of the sintered ceramics was measured by the Archimedes liquid immersion technique. Structural characterization of samples was carried out by X'pert Pro X-ray diffraction (XRD) using Cu Kα radiation (wavelength = 0.154056 nm), with acceleration voltage of 40 kV and current of 40 mA. The fractured morphology of ceramics was observed by JEOL 6360 scanning electron microscope (SEM). Elemental composition of ceramics was evaluated by energy-dispersive X-ray spectroscopy (EDS) performed on Oxford INCA equipment. The electrical resistivity of ceramics was analyzed by four-point probe method.

3 Results

3.1 Densification behavior

The linear shrinkage of ceramics was measured using the following formula [22]:

$$L = \frac{l_0 - l_1}{l_0} \times 100\,\% \quad (1)$$

where L is the linear shrinkage; l_0 and l_1 are the diameter of ceramics before and after the sintering process, respectively.

The linear shrinkage and relative density of AZO ceramics (denoted as L_{AZO} and R_{AZO}, respectively) sintered at 1350 °C increase and then decrease with holding time, both with a peak at 4 h (Fig. 1a).

For further information on multiple comparisons, Fig. 1b shows the linear shrinkage (L_{AZO} and L_{ABZO}) and relative density (R_{AZO} and R_{ABZO}) of AZO and ABZO ceramics as a function of sintering temperature with 4 h of holding time. It can be seen that the L_{AZO} and R_{AZO} of AZO ceramics increase slowly along with the sintering temperature and reach the maximum values of 13.61 % of L_{AZO} and 99.01 % of R_{AZO} at 1350 °C, then decline to 13.42 % of L_{AZO} and 94.87 % of R_{AZO} at 1400 °C, respectively. Hence, it can be concluded from this result that the sintering temperature of 1350 °C with 4 h of holding time used in this present work is appropriate for pores removal and crystallization process of the green bodies to obtain the desired dense AZO ceramics.

Differently, the L_{ABZO} and R_{ABZO} of ABZO ceramics increase very rapidly with increasing sintering temperature (Fig. 1b). The 13.69 % of L_{ABZO} and 97.65 % of R_{ABZO} of ABZO ceramic are obtained at 900 °C, which are observed to be further increased but very slowly, reaching the

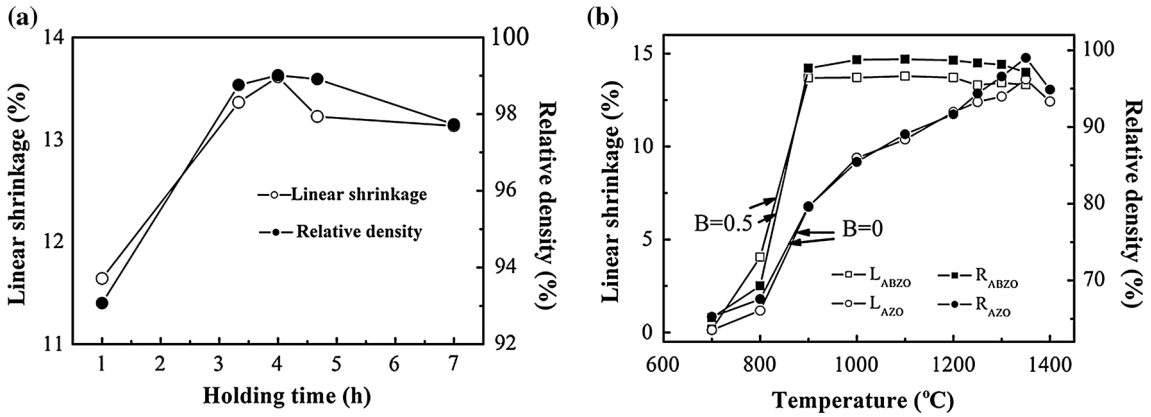

Fig. 1 Linear shrinkage and relative density versus **a** holding time of AZO ceramics sintered at 1350 °C and **b** sintering temperature of AZO and ABZO ceramics with holding time of 4 h

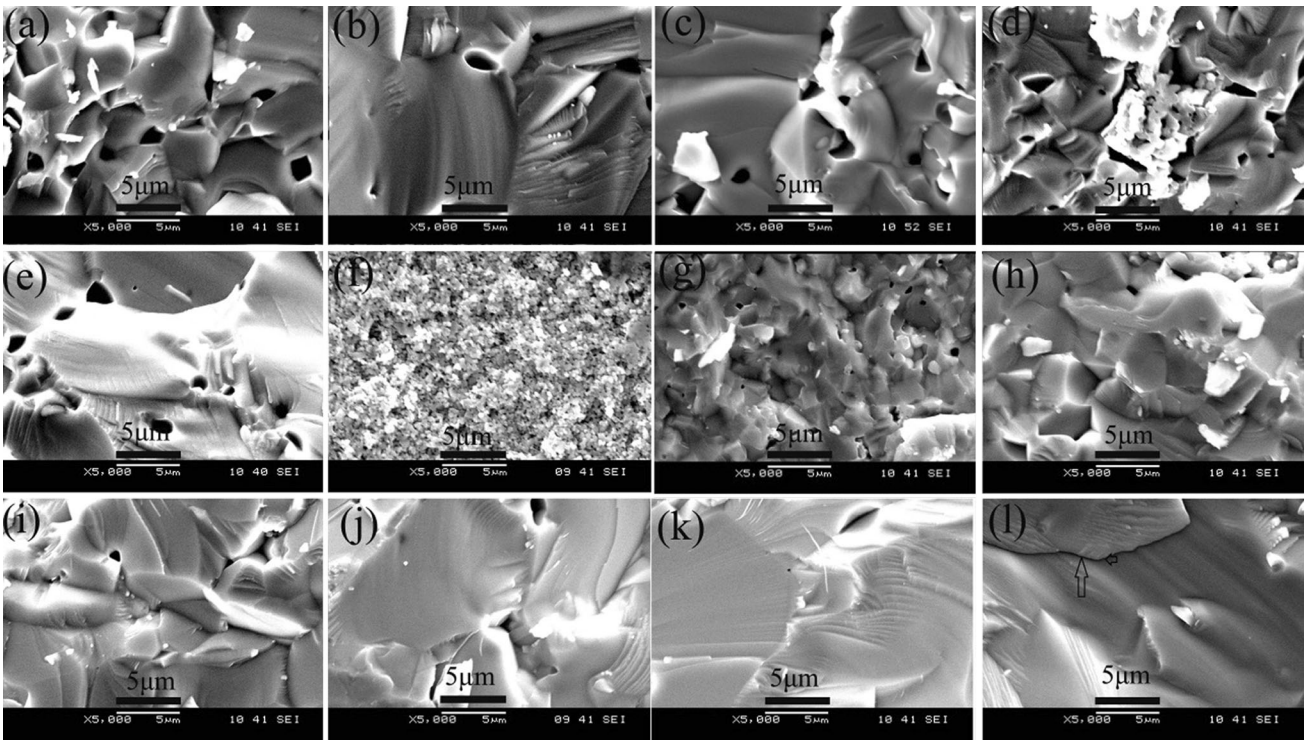

Fig. 2 SEM micrographs ceramics of **a** AZO, 1350 °C, 1 h; **b** AZO, 1350 °C, 4 h; **c** AZO, 1350 °C, 7 h; **d** AZO, 1300 °C, 4 h; **e** AZO, 1400 °C, 4 h; **f** ABZO, 800 °C; **g** ABZO, 900 °C; **h** ABZO, 1000 °C; **i** ABZO, 1100 °C; **j** ABZO, 1200 °C; **k** ABZO, 1300 °C; **l** ABZO, 1350 °C. All ABZO ceramics were sintered with holding time of 4 h

maximum value of 13.78 % of L_{ABZO} and 98.84 % of R_{ABZO} at only 1100 °C, and then both decrease slightly.

3.2 SEM observation

Fractured morphologies of AZO and ABZO ceramics are shown in Fig. 2a–l. The AZO ceramics obtained at 1350 °C for 1 h (Fig. 2a) and 1300 °C for 4 h (Fig. 2d) clearly show the existence of many pores and microstructural irregularities, which agrees well with their low relative density. At the sintering temperature of 1350 °C with the holding time for 4 h (Fig. 2b), the pores disappear and the grains grow up accompanying by many grain boundaries, which is the main characteristic of AZO ceramics having the high density. However, for AZO ceramics sintering at 1350 °C with holding time rising up to 7 h (Fig. 2c) or the sintering temperature rising up to 1400 °C with holding time for 4 h (Fig. 2e), the lamellar structure appears accompanied by large pores, which corresponds well with the decreased relative density.

From the SEM images of ABZO ceramics shown in Fig. 2f–l, it is clearly seen that the porosity is quite high after sintering at 800 °C (Fig. 2f), implying the densification is not available, which agrees well with its low sintering density presented in Fig. 1. However, the ABZO ceramics are dark and homogeneous between 900 and 1100 °C, as shown in Fig. 2g–i, in which very few pores are evident, proving that the densification of ABZO ceramics is obvious after sintering above 900 °C. Furthermore, there is no significant structure gradient along the radial direction, and the corresponding grain size of ABZO ceramics increases from 0.8 to 6.2 μm. When the sintering temperature increases to 1200–1300 °C (Fig. 2j, k), the grain boundaries tend to disappear, producing glass-like structure (glassy phase), which makes it difficult to distinguish the single grains from grain boundaries, implying a very homogeneous microstructure. This homogeneous microstructure without grain boundaries could play an important role in the decrease of the carrier scattering among the grains when they are used into an electrode material. Moreover, as the sintering temperature reaches up to 1350 °C, a bimodal structure consisting of supergrain boundaries (as indicated by arrows) accompanied by the glassy phase is observed in Fig. 2l.

3.3 XRD and EDS analysis

Figure 3a, b presents X-ray diffraction (XRD) patterns of AZO ceramics sintered at different sintering temperatures and holding times, respectively. The predominant peaks in XRD patterns of AZO ceramics are attributed to hexagonal wurtzite ZnO [23]. It is obvious that the synthesized AZO ceramics possess considerably high crystallinity, as evidenced by the sharp intensity of most dominant diffraction peaks. The entire diffraction peak positions of AZO ceramics shift toward higher angles compared to that of standard ZnO. Such an increase suggests the lattice shrinkage of ZnO ceramics which was probably due to the ionic radii difference between Zn^{2+} (0.74 Å) and Al^{3+} (0.054 Å), implying that Al^{3+} ions were substituted into Zn^{2+} sites [24]. Additionally, minor amounts of spinel $ZnAl_2O_4$ can be found in the XRD patterns, proving that

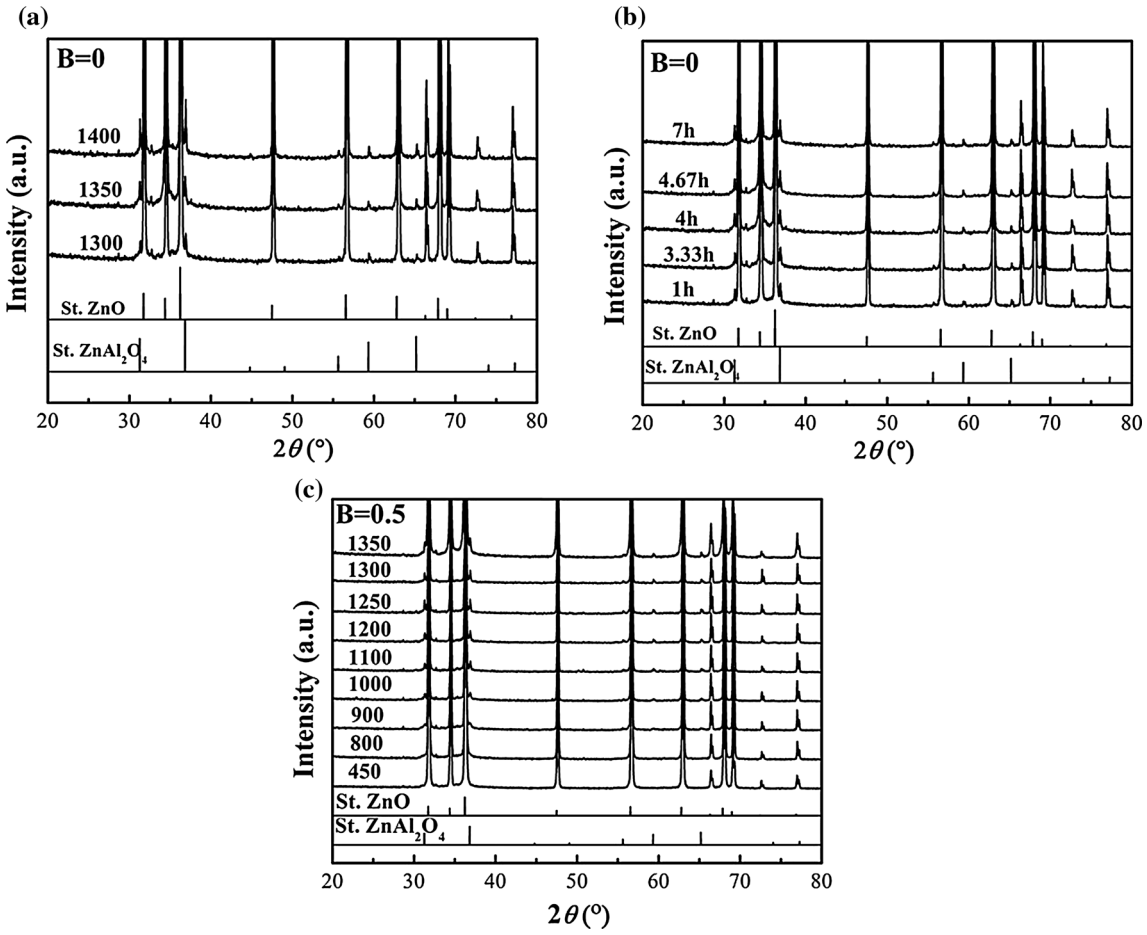

Fig. 3 XRD patterns of **a** AZO ceramics sintered at different temperatures with holding time of 4 h, **b** AZO ceramics sintered at 1350 °C with different holding times and **c** ABZO ceramics sintered at different temperatures with holding time of 4 h

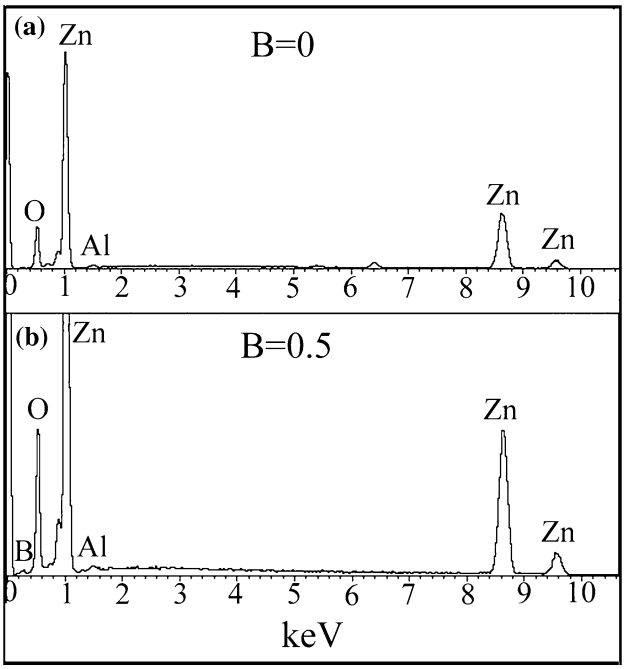

Fig. 4 EDS patters of **a** AZO ceramic sintered at 1350 °C, 4 h, and **b** ABZO ceramic, 1200 °C, 4 h

the sintered AZO ceramics do not consist in a single-phase structure, but a mixed double-phase structure.

Figure 3c shows XRD patterns of ABZO ceramics sintered from 450 to 1350 °C in this present work. There are no peaks of other phases observed except hexagonal ZnO in the XRD patterns from 450 to 900 °C, pointing out that the ABZO ceramics comprise a single crystalline phase without any other impurities. However, the weak diffraction peaks suggesting the presence of $ZnAl_2O_4$ can be observed when the sintering temperature reaches up to 1000 °C. The formation of $ZnAl_2O_4$ phase should be ascribed to the doping concentration beyond the solubility limit of Al in ZnO at high sintering temperatures [25–28]. Similarly, all the entire diffraction peak positions of ABZO ceramics shift toward higher angles compared to that of standard ZnO, implying some Al ions have incorporated into ZnO lattices replacing Zn sites.

In EDS observations for AZO and ABZO samples shown in Fig. 4, Zn, Al, O elements are detected in AZO ceramic and Zn, Al, O, B elements are detected in ABZO ceramic without any other impurities, indicating the sintered ceramics are pure and Al, B have incorporated into ZnO matrix.

3.4 Electrical properties

The electrical resistivity of the ceramics is one of the most important properties in addition to their relative density. Wei et al. [29] suggested that $ZnAl_2O_4$ phase was an electrical

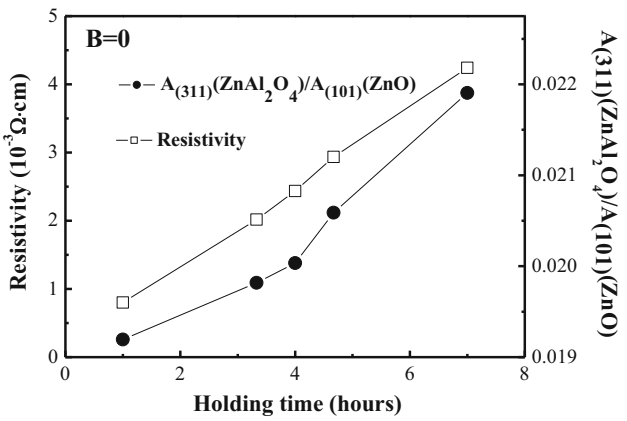

Fig. 5 Electrical resistivity and ratio of $A_{(311)}(ZnAlO_4)/A_{(101)}(ZnO)$ of AZO ceramics sintered at 1350 °C with different holding times

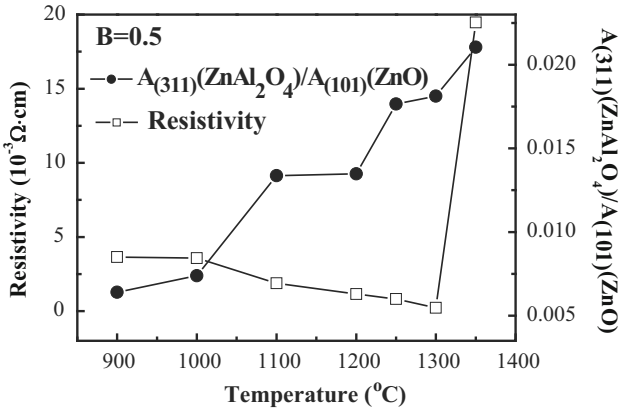

Fig. 6 Electrical resistivity and ratio of $A_{(311)}(ZnAlO_4)/A_{(101)}(ZnO)$ of ABZO ceramics sintered at different temperatures with holding time of 4 h

insulator, which could decrease the electrical conductivity of AZO. Basically, the weight percentage of the $ZnAl_2O_4$ phase can be evaluated from the integrated intensity of the XRD peaks according to the area ratio of the integrated intensity of the strongest $ZnAl_2O_4$ plane reflection to the integrated intensity of the strongest ZnO plane reflection [30]. In this present study, to clarify the effect of $ZnAl_2O_4$ phase on the electrical properties of the sintered ceramics, the area ratios of $(311)_{ZnAl_2O_4}/(101)_{ZnO}$ of the XRD patterns of AZO and ABZO ceramics and their electrical resistivity were investigated, and the result is illustrated in Figs. 5 and 6, respectively. It can be seen that the area ratio of $(311)_{ZnAl_2O_4}/(101)_{ZnO}$ of AZO ceramics increases as the holding time increases monotonously, while the corresponding electrical resistivity increases monotonously too, which indicates the increase in electrical resistivity of AZO ceramics is mainly resulted from the formation of insulated $ZnAl_2O_4$

phase [29]. The $ZnAl_2O_4$ phase could decrease the donor and carrier concentrations, which plays an important role for the deterioration of electrical property of AZO ceramics.

As shown in Fig. 6, the area ratio of $(311)_{ZnAl_2O_4}/(101)_{ZnO}$ of ABZO ceramics increases monotonously from 900 to 1300 °C, but the electrical resistivity decreases with sintering temperature before 1300 °C. Then the electrical resistivity of ABZO ceramics increases about two orders of magnitude up to 1350 °C.

4 Discussion

During sintering, the necks between touching particles formed initially and the pores drifted toward the particle surfaces. Some small particles grew into large grains causing the grain boundaries and pores disappear, which resulted in the shrinkage and density increase of ceramics. A great many of pores existed in AZO ceramics when the holding time was low because of incomplete densification of ceramics. As the holding time increased, the ceramics became dense because the pores disappeared gradually. However, as the holding time exceeded a certain value, the ZnO volatilization occurred which resulted in the pore formation and reduction of the linear shrinkage and relative density [14, 18]. Besides, the new $ZnAl_2O_4$ phase formed with sintering holding time due to the reaction between ZnO and Al_2O_3 as can be proven in the XRD patterns below, which pinned on grain boundaries, reduced the driving force of ceramic densification and consequently decreased the linear shrinkage, relative density and electrical conductivity [6]. The increase in L_{AZO} and R_{AZO} with increasing sintering temperature is mainly related to the pores elimination in the compacts, and the observed reduction of L_{AZO} and R_{AZO} with excessive sintering temperature is related to the ZnO volatilization and $ZnAl_2O_4$ formed in ceramics as mentioned above [6, 14, 18]. Therefore, a fixed value of holding time for 4 h and sintering temperature of 1350 °C would be the satisfactory preparation parameters to obtain AZO ceramics with high density.

The L_{ABZO} and R_{ABZO} of ABZO samples were higher than those of AZO counterparts (before 1300 °C). These earlier densification and high sintering rate suggest that a small amount of boron doping could effectively assist in the sintering densification of AZO ceramics, which basically results from the liquid B_2O_3 (melting point is 450 °C) and the subsequent sintering process driven by diffusive mechanisms, resulting in the simultaneous activation of grain interface migration and pores removal. On the other hand, the slightly decreased L_{ABZO} and R_{ABZO} of ABZO ceramics (beyond 1100 °C) are probably related to the above-mentioned volatilization of ZnO, $ZnAl_2O_4$ formation and the glassy phase formed at high sintering temperatures, which can be confirmed by the XRD and SEM images [22]. The glassy phase exhibits a low density than its crystalline counterpart.

Generally, the electrical resistivity is very complex, which can be influenced by grain boundary scattering, impurity scattering and lattice thermal vibration scattering [31]. Among these contributing factors, the grain boundary scattering is dominant in limiting the mobility and the subsequent electrical resistivity in electrical conductive ceramics [31]. When the sintering temperature increased from 900 to 1300 °C, the electrical resistivity decreases gradually, and the ABZO grain boundaries gradually disappeared, forming more crystallites with the same orientations, which can be modeled as in Fig. 7a, as observed above in the SEM analysis in Fig. 2j, k. This microstructure can induce high carrier mobility as a result of the reduced carrier scattering on grain boundaries [24]. It is known that the grain boundary is much more disordered than inside the grain, which is of crucial importance to hinder the carrier transport and decrease the electrical conductivity of conducting materials. Here, the interconnected crystallites possessing the same orientation without grain boundaries can significantly increase the Hall mobility and reduce the electrical resistivity of ABZO ceramics although non-conductive $ZnAl_2O_4$ phase increased with sintering temperature. It is therefore suggested that the change of electrical resistivity of ABZO ceramics should be mainly affected by Hall mobility due to the microstructure change. And thus, it may be this microstructure change of the sintered ABZO ceramic that, by balancing the effect of the non-conductive $ZnAl_2O_4$ phase, contributes to the decrease in the overall electrical resistivity. Wong et al. [20] also indicated that the Hall mobility was one important factor to decrease the electrical resistivity of B_2O_3-doped ZnO thin films.

However, the disappearance of the grain boundaries obtaining homogeneous microstructure could not be achieved in the case of without using the boron doping in AZO ceramics, resulting in the impossibility of the offsetting process of the increased insulated $ZnAl_2O_4$ phase. Therefore, the influence of the absence of boron doping on local structure ultimately led to the formation of an

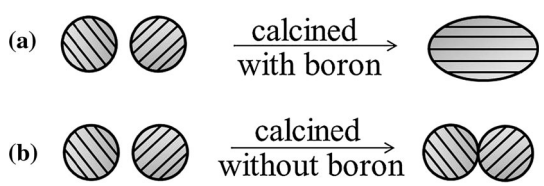

Fig. 7 Schematic diagram of the formation mechanism on structure of **a** ABZO ceramic and **b** AZO ceramic

inhomogeneous microstructure containing crystallites with different orientations, as shown in Fig. 7b. This inhomogeneous microstructure in AZO ceramics ultimately results in the spatial scattering of electron carriers. In addition, the electrical resistivity of ABZO ceramics was significantly increased by increasing the sintering temperature from 1300 to 1350 °C, which corresponds well with the observed supergrain boundaries. The increased electrical resistivity is probably due to the supergrain boundaries formed in the ABZO ceramics which resulted in the serious carrier scattering on grain boundaries and subsequent increase in the overall electrical resistivity. On the other hand, when the sintering temperature increased from 1300 to 1350 °C, the non-conductive $ZnAl_2O_4$ phase rose moderately, as shown in Figs. 3c and 6. This finding shows that after some conductive AZO crystallites have been transformed into non-conductive $ZnAl_2O_4$ phase, the decrease in Al^{3+} donor concentration and increase in carrier scattering by $ZnAl_2O_4$ grain boundaries must occur, which can increase the electrical resistivity of ABZO ceramics. In short, based on the model of the formation mechanism of grain boundary (Fig. 7b), we suggest the possibility that the sharp increased electrical resistivity of ABZO ceramic sintered at 1350 °C is mainly due to the existence of strong carrier scattering on supergrain boundaries because the content of $ZnAl_2O_4$ phase did not increase remarkably from 1300 to 1350 °C. In fact, the ABZO ceramics can achieve a low resistivity by incorporating boron at an appropriate sintering temperature. Thus, it is worth inferring that the dense AZO ceramics with highly crystalline structure and good electrical conductivity can be successfully prepared by the proposed minor boron doping in this present work. The ABZO ceramics with $Al_{1.6}B_{0.5}Zn_{97.9}O$ composition may provide a good option for deposition of high-quality ABZO thin films.

5 Conclusion

AZO and ABZO ceramics with high relative density were successfully prepared. Both the area ratios of $(311)_{ZnAl_2O_4}/(101)_{ZnO}$ and electrical resistivity of AZO ceramics were found to increase with increasing sintering temperature and holding time, respectively. The shift of the diffraction peak positions of AZO and ABZO ceramics toward higher values of 2θ was resulted from the replacement of Zn^{2+} sites by Al^{3+} ions in the ceramics. Al, B co-doped ZnO ceramics were sintered to 98.84 % theoretical density at only 1100 °C, contributing to production costs reduction of ceramics and consequently the costs of optoelectronic applications. The structure of AZO ceramics was inhomogeneous, the electrical resistivity of which increased with $ZnAl_2O_4$ content. Different from that of AZO ceramics, the electrical resistivity of ABZO ceramics decreased with increasing $ZnAl_2O_4$ content probably resulted from the improved microstructure of the ceramics due to boron doping.

Acknowledgements This work was supported by the Natural Science Foundation of Liaoning Province, China (2015020182, 2015020191 and 2015020653), National Natural Science Foundations of China (51472039, 51302024 and 61504017), Program for Liaoning Excellent Talents in University (LR2015010).

References

1. A. Henni, A. Merrouche, L. Telli, A. Azizi, R. Nechache, Mater. Sci. Semicon. Proc. **31**, 380 (2015)
2. J. Lang, J. Wang, Q. Zhang, S. Xu, D. Han, J. Yang, Q. Han, L. Yang, Y. Sui, X. Li, X. Liu, Mater. Sci. Semicon. Proc. **41**, 32 (2016)
3. M. Hjiri, R. Dhahri, K. Omri, L. El Mir, S.G. Leonardi, N. Donato, G. Neri, Mater. Sci. Semicon. Proc. **27**, 319 (2014)
4. M. Yilmaz, Mater. Sci. Semicon. Proc. **40**, 99 (2015)
5. C. Prajapati, P. Sahay, Cryst. Res. Technol. **46**, 1086 (2011)
6. N. Neves, R. Barros, E. Antunes, J. Calado, E. Fortunato, R. Martins, I. Ferreira, J. Eur. Ceram. Soc. **32**, 4381 (2012)
7. I. Miccoli, R. Spampinato, F. Marzo, P. Prete, N. Lovergine, Appl. Surf. Sci. **313**, 418 (2014)
8. J. Xu, Z. Yang, H. Wang, X. Zhang, Bull. Mater. Sci. **37**, 895 (2014)
9. S.H. Nam, M.H. Kim, D.G. Yoo, S.H. Jeong, D.Y. Kim, N.E. Lee, J.H. Boo, Surf. Rev. Lett. **17**, 121 (2010)
10. D. Podobinski, S. Zanin, A. Pruna, D. Pullini, Ceram. Int. **39**, 1021 (2013)
11. Q. Shi, K. Zhou, M. Dai, H. Hou, S. Lin, C. Wei, F. Hu, Ceram. Int. **39**, 1135 (2013)
12. F.H. Hsu, N.F. Wang, Y.Z. Tsai, M.C. Chuang, Y.S. Cheng, M.P. Houng, Appl. Surf. Sci. **280**, 104 (2013)
13. B. Hwang, Y.K. Paek, S.H. Yang, S. Lim, W.S. Seo, K.S. Oh, J. Alloys Compd. **509**, 7478 (2011)
14. J. Zhang, W. Zhang, E. Zhao, H.J. Jacques, Mater. Sci. Semicon. Proc. **14**, 189 (2011)
15. N. Neves, A. Lagoa, J. Calado, A. Botelho Do Rego, E. Fortunato, R. Martins, I. Ferreira, J. Eur. Ceram. Soc. **34**, 2325 (2014)
16. Y. Yang, P. Lan, M. Wang, T. Wei, R. Tan, W. Song, Nanoscale Res. Lett. **7**, 1 (2012)
17. N. Neves, R. Barros, E. Antunes, I. Ferreira, J. Calado, E. Fortunato, R. Martins, J. Am. Ceram. Soc. **95**, 204 (2012)
18. F. Chen, S. Yang, J. Wu, J.A. Galaviz Perez, Q. Shen, J.M. Schoenung, E.J. Lavernia, L. Zhang, J. Am. Ceram. Soc. **98**, 732 (2015)
19. M.W. Wu, Ceram. Int. **38**, 6229 (2012)
20. L.H. Wong, Y.S. Lai, Thin Solid Films **583**, 205 (2015)
21. B. Wen, C.Q. Liu, N. Wang, H.L. Wang, S.M. Liu, W.W. Jiang, W.Y. Ding, W.D. Fei, W.P. Chai, Appl. Phys. A **121**, 1147 (2015)
22. L. Zhang, J. Huang, J. Yang, K. Tang, B. Ren, Y. Hu, L. Wang, L. Wang, Mater. Sci. Semicon. Proc. **42**, 277 (2016)
23. M.W. Wu, P.H. Lai, C.H. Hong, F.C. Chou, J. Eur. Ceram. Soc. **34**, 3715 (2014)
24. H. Cheng, X. Xu, H. Hng, J. Ma, Ceram. Int. **35**, 3067 (2009)
25. T.K. Roy, D. Bhowmick, D. Sanyal, A. Chakrabarti, Ceram. Int. **34**, 81 (2008)
26. A.K. Zak, M.E. Abrishami, W. Majid, R. Yousefi, S. Hosseini, Ceram. Int. **37**, 393 (2011)

27. P.J. Isherwood, N. Neves, J.W. Bowers, P. Newbatt, J. Walls, Thin Solid Films **566**, 108 (2014)
28. A.A.A. Ahmed, Z.A. Talib, M.Z. Bin Hussein, A. Zakaria, J. Solid State Chem. **191**, 271 (2012)
29. T. Wei, Y. Zhang, Y. Yang, R. Tan, P. Cui, W. Song, Surf. Coat. Technol. **221**, 201 (2013)
30. S. Serio, M.E. Melo Jorge, M.J.P. Maneira, Y. Nunes, Mater. Chem. Phys. **126**, 73 (2011)
31. F. Chen, X. Li, J. Wu, Q. Shen, J.M. Schoenung, L. Zhang, Scr. Mater. **68**, 297 (2013)